

Model of dynamic self-assembly in ferromagnetic suspensions at liquid interfacesD. L. Piet,^{1,2} A. V. Straube,³ A. Snezhko,² and I. S. Aranson^{1,2}¹*Department of Engineering Science and Applied Mathematics, Northwestern University, 2145 Sheridan Road, Evanston, Illinois 60208, USA*²*Materials Science Division, Argonne National Laboratory, 9700 South Cass Avenue, Argonne, Illinois 60439, USA*³*Department of Physics, Humboldt University of Berlin, Newtonstraße 15, 12489 Berlin, Germany*

(Received 18 July 2013; published 30 September 2013)

Ferromagnetic microparticles suspended at the interface between immiscible liquids and energized by an external alternating magnetic field show a rich variety of self-assembled structures, from linear snakes to radial asters. In order to obtain insight into the fundamental physical mechanisms and the overall balance of forces governing self-assembly, we develop a modeling approach based on analytical solutions of the time-averaged Navier-Stokes equations. These analytical expressions for the self-consistent hydrodynamic flows are then employed to modify effective interactions between the particles, which in turn are formulated in terms of the time-averaged quantities. Our method allows effective computational verification of the mechanisms of self-assembly and leads to a testable prediction, e.g., on the transitions between various patterns versus viscosity of the solvent.

DOI: [10.1103/PhysRevE.88.033024](https://doi.org/10.1103/PhysRevE.88.033024)

PACS number(s): 47.54.-r, 87.19.ru, 81.16.Dn, 75.50.Tt

I. INTRODUCTION

Dissipative systems exhibit a rich variety of self-organized patterns when they are driven out of equilibrium [1,2]. Colloidal suspensions energized by either external electric or magnetic fields are an important example of mesoscopic, nonequilibrium, pattern-forming systems. Such systems have important technological applications, from photonics to medicine [3,4]. Cross-disciplinary studies on colloidal systems are an ongoing, active area of current research [5–17]. Out-of-equilibrium colloids exhibit a strong propensity towards dynamic self-assembly, which can be defined as a natural tendency of simple building blocks to organize into complex functional architectures. Functionalized colloidal particles, playing the role of these simple building blocks, constitute the basis for new materials via controlled and flexible, bottom-up assembly [18]. One of the most difficult issues in the study of out-of-equilibrium colloids is how collective behavior and ordered dynamic structures arise from discrete particle interactions and what controls the triggering of specific collective responses or desired functionality.

Despite the seeming simplicity, suspensions of ferromagnetic colloidal particles exhibit expansive diversity of dynamic phenomena. Moreover, studies of these suspensions provide insight into dynamic self-assembly of multiparticle systems with strong, long-range anisotropic interactions. An alternating magnetic field is often used to energize the system and trigger the dynamic self-assembly process [19–21]. It was recently demonstrated that a ferromagnetic colloidal suspension confined at the liquid interface and energized by a uniaxial alternating magnetic field applied perpendicular to the interface exhibits nontrivially ordered dynamic structures. These structures range from linear magnetic snakes [19,22,23] observed at a liquid-air interface to radial asters [24] at liquid-liquid interfaces (see Fig. 1). While magnetic snakes are essentially linear structures and comprised of antiferromagnetically ordered segments of ferromagnetically ordered chains of microparticles [19] [Fig. 1(b)], asters exhibit radial structural order with the ferromagnetically ordered chains emanating from the center of each aster [24] [see Fig. 1(c)]. Seemingly

identical systems produce strikingly different self-assembled structures.

To obtain insights into the mechanisms governing dynamic self-assembly phenomena in ferromagnetic suspensions, the shallow water approximation to the Navier-Stokes equations was used in conjunction with Newton's equations of motion for individual particles [25]. The shallow water equations were numerically solved along with Newton's equations, which resulted in the successful modeling of magnetic snakes. In this paper, this approach is further refined by asymptotically solving the shallow water equations in an analytic fashion in lieu of a numerical one. A preliminary account of our work is given in Ref. [26]. These expressions are then inputted directly into Newton's equations for numerical solution. This approach offers several advantages to the one reported in [25], namely, once found, the analytic expressions reveal the overall fluid flow and decay length, giving insight into the forces that cause the dynamic self-assembly. Additionally, bypassing the need for numerical solutions to the shallow water equations greatly reduces the computation time.

On the basis of controlled experiments carried out at the liquid-air interface at different viscosities of the suspending liquid, we have demonstrated that the viscosity defines the intricate balance between magnetic and hydrodynamic forces arising from the inertia of the particles and suspending liquid. The magnitude of these forces is inversely proportional to the viscosity, which can be independently controlled in both our experiment and the theoretical model. We show that at a given frequency and amplitude of the ac magnetic field, the viscosity of the suspending liquid controls the transition between snakes and asters; snakes emerge for smaller viscosities, while asters are favored in more viscous liquids.

II. ANALYTIC MODEL

The analytic model here is the same as that reported briefly in [26] and is comprised of two components, the shallow water equations, which describe the fluid flows induced by particle motion, and the equations governing the interparticle magnetic

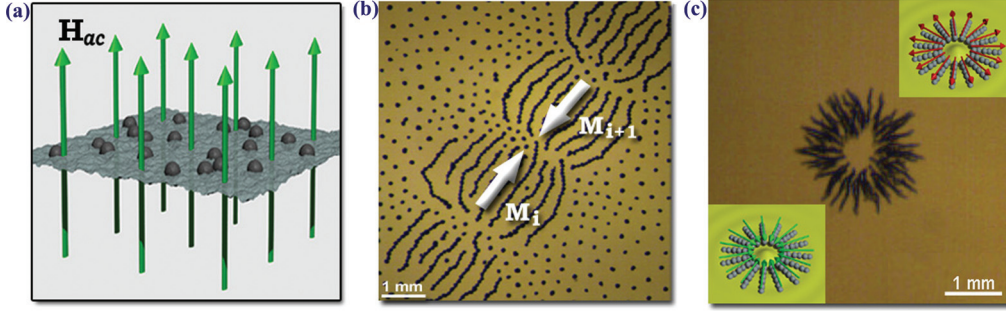


FIG. 1. (Color online) Dynamic self-assembly of ferromagnetic colloidal suspension at liquid interfaces. (a) Schematics of the experiment. An alternating magnetic field is applied perpendicular to the liquid interface supporting the suspension. (b) Self-assembled magnetic snake. Arrows show the direction of the magnetic moments in the segments of the snake. (c) Magnetic aster. The insets demonstrate two equivalent magnetic orderings of asters (aster vs antiaster).

and steric interactions, which are then coupled into Newton's equations for the particle locations and orientations.

A. Governing equations

To model the behavior of the fluid, the shallow water approximation to the Navier-Stokes equations is used, where the fluid is assumed to be incompressible and is considered in the infinite domain $x, y \in (-\infty, \infty)$. The surface elevation $h(\mathbf{r}, t)$ and the two-dimensional (2D) in-plane fluid velocity $\mathbf{v}(\mathbf{r}, t) = (u(\mathbf{r}, t), v(\mathbf{r}, t))$ are described by the equations

$$\frac{\partial h}{\partial t} + \nabla \cdot (h\mathbf{v}) = 0, \quad (1)$$

$$\frac{\partial \mathbf{v}}{\partial t} + (\mathbf{v} \cdot \nabla)\mathbf{v} = \nu_0 \nabla^2 \mathbf{v} - \alpha_0 \mathbf{v} - g \nabla h + \frac{\sigma_0}{\rho} \nabla \nabla^2 h + a_0 \sin(2\pi f t) \sum_j \mathbf{P}_j s(\mathbf{r} - \mathbf{r}_j), \quad (2)$$

where $\nabla = \partial/\partial \mathbf{r}$ is the two-dimensional differential operator of the position vector $\mathbf{r} = (x, y)$, ρ is the fluid density, ν_0 is the kinematic viscosity, σ_0 is the surface tension, g is the gravitational acceleration, and α_0 is the friction with the bottom of the container. The last term in Eq. (2) describes the impact of the particles on the fluid, in which $a_0 \propto H_0$ is the amplitude of the acceleration caused by the magnetic field.

The effective particle in our model has a magnetic moment that always points along the interface of the liquid and as a result represents a short chain (comprised of at least two spherical particles) that produces rocking motion at the liquid interface in the presence of an alternating magnetic field. The response of the chains to the applied magnetic field results in the deformation of the fluid surface (see Fig. 2 in Ref. [25]). The initial formation of short chains of particles is typically justified by the Stokes drag (see, e.g., Ref. [27]) and local deformations of the liquid surface by single spherical particles responding to external driving field [19]. The vectors \mathbf{r}_j and $\mathbf{P}_j = (\cos \phi_j, \sin \phi_j)$ stand for the instant position and orientation of the j th particle, where ϕ_j is the angle of the j th dipole moment. The function $s(\mathbf{r} - \mathbf{r}_j)$ describes the shape of the particles, in our case Dirac delta functions were used, i.e., $s(\mathbf{r} - \mathbf{r}_j) = \delta(\mathbf{r} - \mathbf{r}_j)$. To obtain analytical progress, in our study we neglect the surface tension $\sigma_0 = 0$.

To determine the position and orientation of the particles, Newton's equations of motion are used,

$$m\ddot{\mathbf{r}}_j + \mu_t \dot{\mathbf{r}}_j = \mathbf{F}_j + \mu_t \mathbf{v} - \beta \nabla h, \quad (3)$$

$$I\ddot{\phi}_j + \mu_r \dot{\phi}_j = T_j + \kappa H_0 \sin(\omega t) (\nabla h \times \mathbf{P}_j) \cdot \hat{\mathbf{e}}_z, \quad (4)$$

where m is the particle mass, μ_t is the translational friction, I is the moment of inertia, μ_r is the rotational friction, and \mathbf{F}_j and $\mathbf{T}_j = T_j \hat{\mathbf{e}}_z$ ($\hat{\mathbf{e}}_z$ is the unit vector along the z axis) are the translational and rotational forces due to the interparticle interactions, respectively. The term $\mu_t \mathbf{v}$ is the Stokes drag and $-\beta \nabla h$ ($\beta = mg$) describes the movement along the surface gradient from gravity. The last term in Eq. (4) is the torque applied to the dipole moment resulting from the magnetic field.

The magnetic dipole-dipole \mathcal{U}_{ij}^d and short-range hard-core repulsive \mathcal{U}_{ij}^h interactions are described by the following potentials [28]:

$$\mathcal{U}_{ij}^d = \frac{\mu_d^2}{4\pi r_{ij}^3} [\mathbf{P}_i \cdot \mathbf{P}_j - 3(\mathbf{P}_i \cdot \hat{\mathbf{r}}_{ij})(\mathbf{P}_j \cdot \hat{\mathbf{r}}_{ij})], \quad (5)$$

$$\mathcal{U}_{ij}^h = \frac{\mu_d^2}{16\pi d^3} \left(\frac{d}{r_{ij}} \right)^{24}, \quad (6)$$

where μ_d is the magnetic dipole of the particle, d is the particle diameter, $r_{ij} = |\mathbf{r}_{ij}|$, $\mathbf{r}_{ij} = \mathbf{r}_i - \mathbf{r}_j$, and $\hat{\mathbf{r}}_{ij} = \mathbf{r}_{ij}/r_{ij}$. The translational and rotational forces are evaluated as $\mathbf{F}_j = -\partial \mathcal{U}/\partial \mathbf{r}_j$ and the rotational are $\mathbf{T}_j = -\mathbf{P}_j \times \partial \mathcal{U}/\partial \mathbf{P}_j$, where $\mathcal{U} = (1/2) \sum_{i,j \neq i} \mathcal{U}_{ij}$ and $\mathcal{U}_{ij} = \mathcal{U}_{ij}^d + \mathcal{U}_{ij}^h$.

B. Solution of shallow water equations

We now analyze the shallow water equations (1) and (2). We represent the surface elevation as $h(\mathbf{r}, t) = h_0 + \zeta(\mathbf{r}, t)$, where $\zeta(\mathbf{r}, t)$ describes the deviation of the surface from the equilibrium value h_0 . To address this problem, we pass to dimensionless variables by measuring the length, time, and velocity in units of h_0 , $\sqrt{h_0/g}$, and $\sqrt{g h_0}$, respectively. Setting the surface tension to zero $\sigma_0 = 0$ as mentioned earlier, we arrive at the dimensionless equations

$$\frac{\partial \zeta}{\partial t} = -\nabla \cdot (\mathbf{v} + \zeta \mathbf{v}), \quad (7a)$$

$$\frac{\partial \mathbf{v}}{\partial t} + (\mathbf{v} \cdot \nabla)\mathbf{v} = \nu(\nabla^2 \mathbf{v} - \alpha \mathbf{v}) - \nabla \zeta + \epsilon \sin \omega t \sum_j \mathbf{P}_j \delta(\mathbf{r} - \mathbf{r}_j), \quad (7b)$$

with the dimensionless frequency $\omega = 2\pi f\sqrt{h_0/g}$, viscosity $\nu = \nu_0/h_0\sqrt{gh_0}$, friction with the bottom of the container $\alpha = \alpha_0 h_0^2/\nu_0$, and strength of external driving $\epsilon = a_0(H_0)/g$, which is the acceleration caused by the magnetic field measured relative to g .

Note that in the case of no external driving, when $\epsilon = 0$, the liquid subsystem has no source of motion. In particular, in Appendix A we show that the linearized system admits damped surface gravity waves, as ensured by the viscous dissipation in the bulk and additionally via the friction with the bottom of the container. As a result, any initial perturbation decays and the liquid system tends to the equilibrium state with $\mathbf{v}(\mathbf{r}, t) \rightarrow 0$ and $\zeta(\mathbf{r}, t) \rightarrow 0$ as $t \rightarrow \infty$ for all \mathbf{r} .

We now focus on the case of weak external driving $\epsilon \ll 1$, which at the same time implies that the surface deformations induced by the particles driven by the magnetic field are small $\zeta \ll 1$ (or $\zeta \ll h_0$ in the units before rescaling). This consideration suggests the perturbation ansatz

$$\zeta(\mathbf{r}, t) = \epsilon \zeta_1(\mathbf{r}, t) + \epsilon^2 \zeta_2(\mathbf{r}, t) + O(\epsilon^3), \quad (8a)$$

$$\mathbf{v}(\mathbf{r}, t) = \epsilon \mathbf{v}_1(\mathbf{r}, t) + \epsilon^2 \mathbf{v}_2(\mathbf{r}, t) + O(\epsilon^3). \quad (8b)$$

Here the leading terms of $O(\epsilon)$ describe the linear response of the system, which can be used to compute the mean flow by performing the time averaging of equations in the next order $O(\epsilon^2)$, as described below.

1. First-order solution: Linear response

As shown in Appendix B 1, by applying the ansatz (8) to Eqs. (7) at the leading order we arrive at the linear equations, which can be solved in the far-field approximation for small viscosity. The leading parts of the general solutions in terms of complex amplitudes are given by Eqs. (B8)–(B11). For the velocity fields and the surface deviation generated by a single particle j , we have

$$u_1(\mathbf{r}, t) = \frac{\sqrt{\omega} e^{-\nu\gamma R_j} \cos \chi_j \cos(\varphi_j - \theta_j) \cos \theta_j}{2\sqrt{2\pi R_j}}, \quad (9)$$

$$v_1(\mathbf{r}, t) = \frac{\sqrt{\omega} e^{-\nu\gamma R_j} \cos \chi_j \cos(\varphi_j - \theta_j) \sin \theta_j}{2\sqrt{2\pi R_j}}, \quad (10)$$

$$\zeta_1(\mathbf{r}, t) = \frac{e^{-\nu\gamma R_j} \cos(\varphi_j - \theta_j)}{4\sqrt{2\pi\omega} R_j^{3/2}} (2k_0 R_j \cos \chi_j + \sin \chi_j). \quad (11)$$

Note that the fields are represented relative to the time-averaged position \mathbf{q}_j of particle j such that $\mathbf{R}_j := \mathbf{r} - \mathbf{q}_j = R_j(\cos \theta_j, \sin \theta_j)$ and $\chi_j = k_0 R_j + \pi/4 - \omega t$. Here θ_j is the angle between the vector \mathbf{R}_j and the reference axis, φ_j is the angle that determines the time-averaged orientation of the dipole moment, and the coefficients k_0 and γ are determined by the dispersion relation [see Eq. (A2)].

Also note that these expressions diverge as $\mathbf{R}_j \rightarrow 0$, which is a direct result of using δ functions to model the spatial extension of the particles [see Eq. (2)]. This singularity does not present a problem since the hard-core magnetic repulsion from Eq. (6) keeps the interparticle separation distances large enough where this divergence is never felt. The first-order velocity field \mathbf{v}_1 and surface deformation ζ_1 produced by a single particle, as given in Eqs. (9)–(11), are shown in Figs. 2(a) and 2(b), respectively.

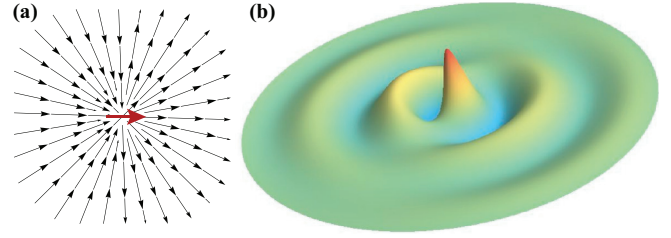


FIG. 2. (Color online) (a) Instant first-order velocity field induced by a single particle. The red (large center) arrow indicates the location and direction of the dipole moment. (b) First-order surface deformation where the color code (grayscale) denotes the surface height. Note that both the velocities and the surface deformation decay exponentially.

2. Second-order solution: Mean flow

In Appendix B 2 we apply the ansatz (8) to Eqs. (7) to obtain the mean flow produced by a single particle. The second-order equations are averaged over time and the mean velocity \mathbf{u}_j produced by particle j is represented in terms of the velocity potential $\Phi_j(\mathbf{r})$ and stream function $\Psi_j(\mathbf{r})$, $\mathbf{u}_j = \nabla \Phi_j + (\hat{\mathbf{e}}_z \times \nabla \Psi_j)$. These functions are given by Eqs. (B18) and (B19). Both the curl-free and divergence-free counterparts of the mean flow determined by the potential $\Phi(\mathbf{r})$ and stream function $\Psi(\mathbf{r})$, as in Eqs. (B18) and (B19), have long-range quadrupolar structures that decay like $1/r^3$, shown in Figs. 3(a) and 3(b), respectively. The combined net mean flow is presented in Fig. 3(c). As was observed experimentally, the long-range quadrupolar flow was an essential ingredient for the formation of snakes and asters. Additionally, a comparison of the decay length between first-order and time-averaged (mean) second-order flows is shown in Fig. 3(d).

C. Time-averaged equations for the motion of particles

As shown in Appendix C 1, based on the analytic solutions of the shallow water equations discussed in Sec. II B and in Appendix B, we can formulate effective equations for the time-averaged motion of particles, which can be formulated in closed form and do not require solution of the Navier-Stokes equations. Thus, instead of the initial model, given by Eqs. (1) and (2) for the solvent and Eqs. (3) and (4) for the particles, we describe the same system with only three equations per particle, two for the 2D position $\mathbf{q}_j(t)$ and one for the orientation $\varphi_j(t)$. All of the details about the complex long-range hydrodynamic flows are cast in pairwise interactions:

$$m\ddot{\mathbf{q}}_j + \mu_t \dot{\mathbf{q}}_j = \mathbf{F}_j + \mu_t \mathbf{u}(\mathbf{q}_j, t) + \mathbf{s}(\mathbf{q}_j), \quad (12)$$

$$I\ddot{\varphi}_j + \mu_r \dot{\varphi}_j = T_j + \kappa H_0 [\nabla H(\mathbf{q}_j) \times \mathbf{P}_j] \cdot \hat{\mathbf{e}}_z. \quad (13)$$

Here the forces \mathbf{F}_j and torques T_j are to be evaluated based on the time-averaged positions \mathbf{q}_j ; the mean flow field $\mathbf{u}(\mathbf{q}_j)$ and the Stokes drift given by the superposition $\mathbf{s}(\mathbf{q}_j) = \mathbf{s}^{(S)}(\mathbf{q}_j) + \mathbf{s}^{(G)}(\mathbf{q}_j)$ are determined by Eqs. (C6) and (C10)

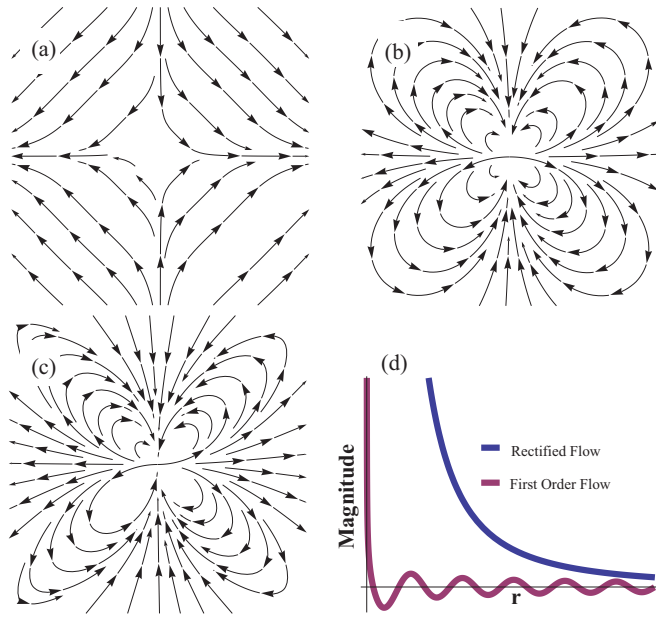


FIG. 3. (Color online) Mean flow field broken into its constituents along with a comparison of the first-order velocity to the second-order velocity: (a) the quadrupolar potential flow, (b) the quadrupolar vorticity flow, and (c) the composite of potential and vorticity flow. (d) Velocity profiles of the first-order and time-independent mean flow as a function of distance from the particle. The first-order solution oscillates and decays exponentially, whereas the mean flow is monotonic and decays like $1/r^3$.

together with expressions (C7) and (C11). The time-averaged quantity $H(\mathbf{q}_j)$ in Eq. (13) is given by formula (C13).

III. NUMERICAL SIMULATIONS

To model the experimentally observed self-assembly of magnetic particles, we performed numerical simulations of Eqs. (12) and (13), using a simple Verlet integration method. The simulations were run on a high-performance NVIDIA GPU cluster. By varying the frequency of the applied field and the viscosity of the suspending fluid, both snakes and asters were reproduced. Figures 4 and 5 show snake and aster formations respectively, wherein 225 particles were dispersed in a rectangular (snake) or square (aster) domain. In this domain the dipole orientations were uniformly distributed and particles were placed on the square lattice with small random displacements. After a short period, the self-assembly process was complete and yielded one of the two phases.

Moreover, this model successfully reproduced the phase diagram between snakes and asters as a function of fluid viscosity η and frequency f [26]. As shown in the top panel of Fig. 3 of [26], the crossover in the self-assembly behavior is illustrated, displaying a staggering similarity to the experimental one in the top panel of Fig. 1 of [26]. Note that here, $\alpha = \rho = 1$. The dependence of a characteristic structure formation time for the self-assembly process on η exhibits a trend also similar to that in the experimental case [26]. Note

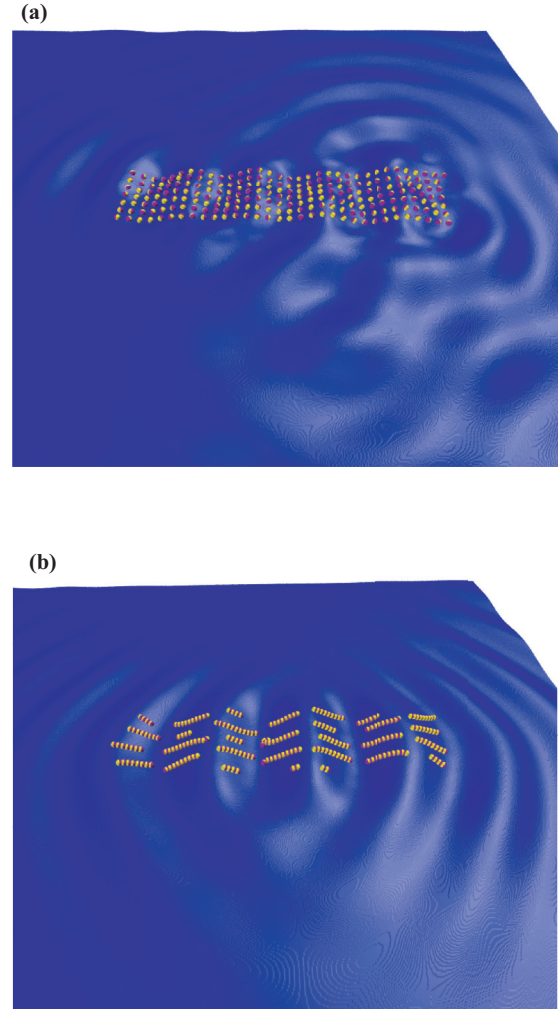


FIG. 4. (Color online) Snake formation. (a) Two hundred twenty-five particles are initially dispersed in a rectangular domain. (b) A snake is formed by the ferromagnetic chains aligned side by side to make snake segments along the surface gradient that are antiferromagnetically aligned with their neighboring segments.

that, in order to avoid depth dependence, the axes in the top panel of Fig. 3 of [26] remain in dimensionless quantities.

As it was shown in [26], this approach made it possible to recover the two primary experimental phases of snakes and asters. Though it was unexpected for asters to appear because of the 3D toroidal flows they induce, it was revealed that formation of these structures is a product of surface deformation rather than fluid flow. This conclusion would not have been made had it not been for the alternative solution methods performed here.

IV. CONCLUSION

Our previous experimental and theoretical studies revealed that long-range (and highly nonlinear in nature) rectified (mean) flow and inertia of the particles are crucial for the formation of asters and snakes. Here we have demonstrated that a relatively simple model for interacting particles can successfully describe a variety of self-assembled structures

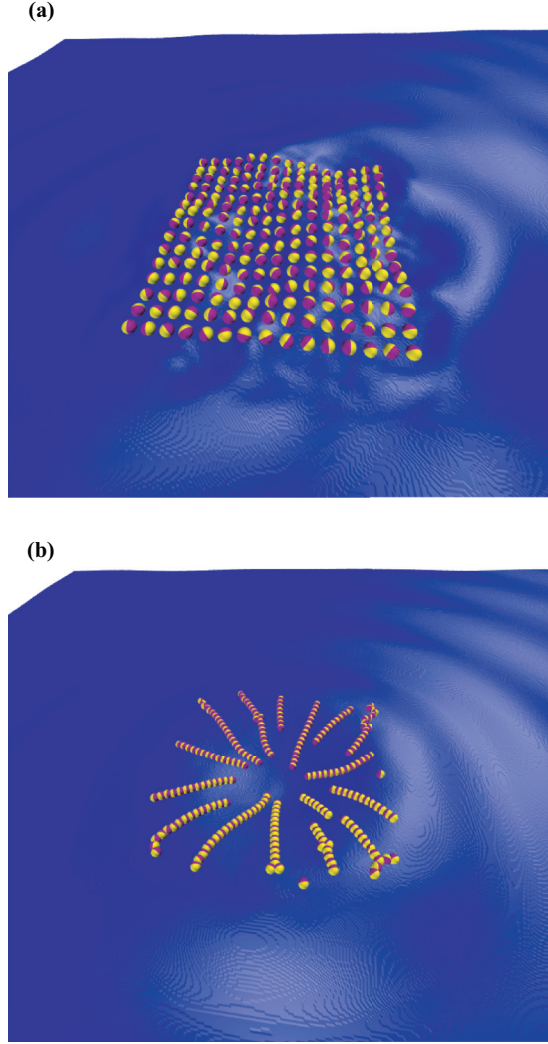


FIG. 5. (Color online) Aster formation. (a) Two hundred twenty-five particles are initially dispersed in a square domain. (b) An aster is formed by an axisymmetric ordering of ferromagnetic chains aligned along the induced surface gradient.

formed at the interface between immiscible liquids. A crucial ingredient of our approach is that in order to reproduce primary self-assembled patterns, such as snakes and asters, standard interparticle interactions, e.g., steric repulsion and dipolar, have to be supplemented by the self-consistent hydrodynamic flows. Analytical solutions of the time-averaged Navier-Stokes equations allow formulation of these flows in an explicit form. In this regard our work exemplifies how well-established discrete particle methods, e.g., Brownian dynamics [4], can be extended in order to include nonlinear fluid-mediated interactions between the particles. The success of our modeling approach is further illustrated by a testable prediction on the transition between asters and snakes as a function of the viscosity of suspending liquid. Our modeling framework can possibly be extended towards other out-of-equilibrium self-assembled systems where self-induced hydrodynamic flows play a critical role in the interparticle interactions.

ACKNOWLEDGMENTS

The research was supported by the US DOE, Office of Basic Energy Sciences, Division of Materials Science and Engineering, under the Contract No. DE AC02-06CH11357. A.V.S. thanks Argonne's Materials Theory Institute for support of his visit to Argonne.

APPENDIX A: CALCULATING THE DISPERSION RELATION

Here we consider the dispersion relation, which can be obtained from the (linear) first-order equations in the case of no external driving [see Eqs. (B3) and (B4)]. Using Eq. (B3) to eliminate $\hat{\xi}$ in Eq. (B4), multiplying the result by $-i\omega$, and setting $\mathbf{P}_j = 0$ yields

$$\omega^2 \hat{\mathbf{V}} = -i\nu\omega(k^2 + \alpha)\hat{\mathbf{V}} + \mathbf{k}(\mathbf{k} \cdot \hat{\mathbf{V}}),$$

which presents a linear homogeneous system of a pair of algebraic equations with respect to \hat{U} and \hat{V} . This system admits a nontrivial solution only if its determinant turns to zero. Building the corresponding characteristic equation gives us the desired dispersion relation

$$\mathcal{D}(\omega, k, \nu, \alpha) = 0$$

with the function

$$\mathcal{D} = [\omega^2 - k^2 - i\nu\omega(k^2 + \alpha)][\omega - i\nu(k^2 + \alpha)]. \quad (\text{A1})$$

In the limiting case of inviscid liquid $\nu = 0$, the dispersion relation reduces to the conventional result known for shallow water $\omega = \pm k$ or, equivalently, $\omega = \pm\sqrt{gh_0}k$ in the original units before rescaling. For arbitrary ν , no analytical solution is available. We are, however, interested in the case of small viscosity ν , in which we obtain an approximation

$$k \approx k_0 - i\nu\gamma, \quad k_0 = \omega, \quad \gamma = \frac{\omega^2 + \alpha}{2}. \quad (\text{A2})$$

Here k_0 is the inviscid contribution describing the gravity waves at the surface of shallow water and γ is a viscous damping coefficient responsible for their damping.

APPENDIX B: CALCULATING THE ASYMPTOTIC SOLUTIONS FOR THE SHALLOW WATER EQUATIONS

1. First-order solution: Linear response

Here we deal with the linear response of the system. Applying the ansatz (8) to Eqs. (7) and retaining the leading terms, we arrive at the first-order equations

$$\frac{\partial \zeta_1}{\partial t} = -\nabla \cdot \mathbf{v}_1, \quad (\text{B1})$$

$$\frac{\partial \mathbf{v}_1}{\partial t} = \nu(\nabla^2 \mathbf{v}_1 - \alpha \mathbf{v}_1) - \nabla \zeta_1 + \sin \omega t \sum_j \bar{\mathbf{P}}_j \delta(\mathbf{r} - \mathbf{q}_j), \quad (\text{B2})$$

with \mathbf{q}_j and $\bar{\mathbf{P}}_j = (\cos \varphi_j, \sin \varphi_j)$ being the time-averaged position and orientation of particle j , respectively [see also representation (C1)]. We now pass to complex amplitudes $\zeta_1(\mathbf{r}, t) = \xi(\mathbf{r})e^{i\omega t} + \text{c.c.}$ and $\mathbf{v}_1(\mathbf{r}, t) = \mathbf{V}(\mathbf{r})e^{i\omega t} + \text{c.c.}$ in Eqs. (B1) and (B2), where $\mathbf{V}(\mathbf{r}) = (U(\mathbf{r}), V(\mathbf{r}))$ and c.c.

denotes the complex conjugate. Then the amplitudes $\xi(\mathbf{r})$ and $\mathbf{V}(\mathbf{r})$ are transformed into Fourier space, using the convention

$$\mathcal{F}(\mathbf{r}) = \frac{1}{2\pi} \int_{\mathbb{R}^2} \hat{\mathcal{F}}(\mathbf{k}) e^{i\mathbf{k}\cdot\mathbf{r}} d\mathbf{k}, \quad \hat{\mathcal{F}}(\mathbf{k}) = \frac{1}{2\pi} \int_{\mathbb{R}^2} \mathcal{F}(\mathbf{r}) e^{-i\mathbf{k}\cdot\mathbf{r}} d\mathbf{r},$$

to arrive at the algebraic equations

$$i\omega\hat{\xi} = -i(\mathbf{k} \cdot \hat{\mathbf{V}}), \quad (\text{B3})$$

$$i\omega\hat{\mathbf{V}} = -\nu(k^2 + \alpha)\hat{\mathbf{V}} - i\mathbf{k}\hat{\xi} + \frac{1}{4\pi i} \sum_j \bar{\mathbf{P}}_j e^{-i\mathbf{k}\cdot\mathbf{q}_j}, \quad (\text{B4})$$

where $\mathbf{k} = (k_x, k_y)$ and $k^2 = k_x^2 + k_y^2$. Equations (B3) and (B4) are then solved for the velocity field $\hat{\mathbf{V}}(\mathbf{k}) = (\hat{U}(\mathbf{k}), \hat{V}(\mathbf{k}))$, giving

$$\hat{U}(\mathbf{k}) = \sum_j \frac{[k_y^2 - \omega^2 + i\nu\omega(k^2 + \alpha)]\bar{P}_j^x - k_x k_y \bar{P}_j^y}{4\pi \mathcal{D}(\omega, k, \nu, \alpha)} e^{-i\mathbf{k}\cdot\mathbf{q}_j},$$

$$\hat{V}(\mathbf{k}) = \sum_j \frac{[k_x^2 - \omega^2 + i\nu\omega(k^2 + \alpha)]\bar{P}_j^y - k_x k_y \bar{P}_j^x}{4\pi \mathcal{D}(\omega, k, \nu, \alpha)} e^{-i\mathbf{k}\cdot\mathbf{q}_j},$$

where the function $\mathcal{D}(\omega, k, \nu, \alpha)$ is determined by Eq. (A1).

To transform these solutions back to the real space we stick to the polar representation of the wave vector $\mathbf{k} = k(\cos\theta_k, \sin\theta_k)$ and the radius vector with the origin at the position of j th particle, $\mathbf{R}_j := \mathbf{r} - \mathbf{q}_j = R_j(\cos\theta_j, \sin\theta_j)$. Integrating over θ_k from 0 to 2π and over k from 0 to ∞ , we can represent the complex amplitudes in the real space as

$$U(\mathbf{r}) = -\frac{1}{8\pi} \sum_j [\mathcal{I}_1(R_j) \cos\varphi_j + \mathcal{I}_2(R_j) \cos(2\theta_j - \varphi_j)],$$

$$V(\mathbf{r}) = -\frac{1}{8\pi} \sum_j [\mathcal{I}_1(R_j) \sin\varphi_j + \mathcal{I}_2(R_j) \sin(2\theta_j - \varphi_j)],$$

where

$$\mathcal{I}_1(r) = \int_0^\infty \frac{2\omega^2 - k^2 - 2i\nu\omega(k^2 + \alpha)}{\mathcal{D}(\omega, k, \nu, \alpha)} k J_0(kr) dk, \quad (\text{B5})$$

$$\mathcal{I}_2(r) = \int_0^\infty \frac{-k^3 J_2(kr) dk}{\mathcal{D}(\omega, k, \nu, \alpha)}. \quad (\text{B6})$$

The critical component of finding the first-order solution to this model is the computation of the integrals in Eqs. (B5) and (B6), particularly at large arguments since these contributions are responsible for the description of the large scale flows. The integral in Eq. (B5) has the analytic solution

$$\mathcal{I}_1(r) = \frac{i}{\nu} K_0(rz) + \frac{\omega}{1 + i\nu} \frac{i\pi}{2} H_0^{(2)}(y_r r) e^{y_i r},$$

with $z = \sqrt{\alpha + i\omega/\nu}$ and $y = \sqrt{\omega(\omega - i\nu)/(1 + i\nu\omega)} = y_r + iy_i$. Note that at small viscosity ν , $y \approx k_0 - i\nu\gamma$ with k_0 and γ following from the dispersion relation at small ν [see Eq. (A2)]. Furthermore, considering large values of r , this expression can be approximated as

$$\mathcal{I}_1(r) \approx -\sqrt{\frac{\pi\omega}{2}} \frac{1}{\sqrt{r}} e^{-\nu\gamma r} e^{-i(k_0 r + \pi/4)}. \quad (\text{B7})$$

For Eq. (B6), no such closed form was found. Instead, the first suitable approximation made is to consider the case for

small viscosities, which is in fact the case in experiment. Then

$$\begin{aligned} \mathcal{I}_2(r) &\approx -\frac{1}{\omega} \int_0^\infty \frac{k^3 J_2(kr) dk}{\omega^2 - k^2 - i\nu\omega(k^2 + \alpha)} \\ &\approx -\omega \frac{i\pi}{2} H_2^{(2)}(k_0 r) e^{-\nu\gamma r}. \end{aligned}$$

This result is then reduced by considering the asymptotic approximation for large arguments, which yields the same result as in Eq. (B7). Thus, for small ν in the far-field approximation, $\mathcal{I}_1(r) = \mathcal{I}_2(r)$ and we obtain the complex amplitudes

$$U(\mathbf{r}) = \sum_j \frac{\sqrt{\omega} e^{-i(kR_j + \pi/4)} \cos(\varphi_j - \theta_j) \cos\theta_j}{4\sqrt{2\pi} R_j}, \quad (\text{B8})$$

$$V(\mathbf{r}) = \sum_j \frac{\sqrt{\omega} e^{-i(kR_j + \pi/4)} \cos(\varphi_j - \theta_j) \sin\theta_j}{4\sqrt{2\pi} R_j}, \quad (\text{B9})$$

in which $k = k_0 - i\nu\gamma$.

The amplitude of the surface deviation can be evaluated as $\xi(\mathbf{r}) = \omega^{-1} \nabla \cdot \mathbf{V}(\mathbf{r})$ [see Eq. (B1)]. Further, we will also need the first-order vorticity field $\Omega_1 = \Omega_1 \hat{\mathbf{e}}_z = \nabla \times \mathbf{v}_1$ and $\Omega_1(\mathbf{r}, t) = \Omega(\mathbf{r}) e^{i\omega t} + \text{c.c.}$ with the complex amplitude $\Omega(\mathbf{r}) = \hat{\mathbf{e}}_z \cdot \nabla \times \mathbf{V}(\mathbf{r})$. Using Eqs. (B8) and (B9), we find for the complex amplitudes

$$\xi(\mathbf{r}) = \sum_j \frac{e^{-i(kR_j + \pi/4)} (i + 2kR_j) \cos(\varphi_j - \theta_j)}{8\sqrt{2\pi} \omega R_j^{3/2}}, \quad (\text{B10})$$

$$\Omega(\mathbf{r}) = \sum_j \frac{\sqrt{\omega} e^{-i(kR_j + \pi/4)} \sin(\varphi_j - \theta_j)}{4\sqrt{2\pi} R_j^{3/2}}. \quad (\text{B11})$$

2. Second-order solution: Time-averaged equations

In this section we consider the second-order equations. By performing the averaging over time, we obtain the equations that describe the long-range mean flow produced by periodically driven particles. The first- and second-order solutions for the motion of liquid are then used to obtain the effective time-averaged equations for the particles.

Applying the ansatz (8) to Eqs. (7), to second order we obtain

$$\frac{\partial \zeta_2}{\partial t} = -\nabla \cdot (\mathbf{v}_2 + \zeta_1 \mathbf{v}_1),$$

$$\frac{\partial \mathbf{v}_2}{\partial t} + (\mathbf{v}_1 \cdot \nabla) \mathbf{v}_1 = \nu(\nabla^2 \mathbf{v}_2 - \alpha \mathbf{v}_2) - \nabla \zeta_2.$$

To calculate the mean flow, we perform the time averaging of the above equations and look for the stationary solution, which satisfies the equations

$$\nabla \cdot \mathbf{u} = -\nabla \cdot (\overline{\zeta_1 \mathbf{v}_1}), \quad (\text{B12})$$

$$\overline{(\mathbf{v}_1 \cdot \nabla) \mathbf{v}_1} = \nu(\nabla^2 \mathbf{u} - \alpha \mathbf{u}) - \nabla \overline{\zeta_2}, \quad (\text{B13})$$

where the overline means the time averaging and the time-averaged second-order velocity field is for simplicity denoted by $\mathbf{u} := \overline{\mathbf{v}_2}$.

We make use of the Helmholtz decomposition of the mean velocity $\mathbf{u} = \nabla \Phi + (\hat{\mathbf{e}}_z \times \nabla \Psi)$ to separate Eqs. (B12) and (B13) into the curl-free and divergence-free contributions, determined by the velocity potential Φ and the stream function Ψ , respectively. We rewrite the nonlinear term in Eq. (B13) as

$\mathbf{v}_1 \cdot \nabla \mathbf{v}_1 = \nabla(v_1^2/2) + \Omega_1 \times \mathbf{v}_1$. To eliminate gradient terms, we apply the curl to Eq. (B13) and project the result onto the z axis. Rewriting everything in terms of the scalar potentials and vorticity, Eqs. (B12) and (B13) decouple and give

$$\nabla^2 \Phi = -\nabla \cdot (\overline{\zeta_1 \mathbf{v}_1}), \quad (\text{B14})$$

$$\nu(\nabla^4 \Psi - \alpha \nabla^2 \Psi) = \nabla \cdot (\overline{\Omega_1 \mathbf{v}_1}). \quad (\text{B15})$$

Next we assume that the contribution from the biharmonic operator in Eq. (B15) is small and therefore dropped from further calculations. Equations (B14) and (B15) are then solved using the Green's function approach, which leads us to formal solutions

$$\Phi(\mathbf{r}) = -\frac{1}{2\pi} \int_{\mathbb{R}^2} \ln|\mathbf{r} - \mathbf{r}'| \nabla' \cdot (\overline{\zeta_1 \mathbf{v}_1}) d\mathbf{r}',$$

$$\Psi(\mathbf{r}) = -\frac{1}{2\pi\nu\alpha} \int_{\mathbb{R}^2} \ln|\mathbf{r} - \mathbf{r}'| \nabla' \cdot (\overline{\Omega_1 \mathbf{v}_1}) d\mathbf{r}',$$

where $\nabla' = \partial/\partial\mathbf{r}'$.

Integrating by parts, we rewrite these expressions to obtain

$$\Phi(\mathbf{r}) = -\frac{1}{2\pi} \int_{\mathbb{R}^2} \frac{(\overline{\zeta_1 \mathbf{v}_1}) \cdot (\mathbf{r} - \mathbf{r}')}{(\mathbf{r} - \mathbf{r}')^2} d\mathbf{r}', \quad (\text{B16})$$

$$\Psi(\mathbf{r}) = -\frac{1}{2\pi\nu\alpha} \int_{\mathbb{R}^2} \frac{(\overline{\Omega_1 \mathbf{v}_1}) \cdot (\mathbf{r} - \mathbf{r}')}{(\mathbf{r} - \mathbf{r}')^2} d\mathbf{r}'. \quad (\text{B17})$$

The time-averaged quantities in the integrals are evaluated via the complex amplitudes as $\overline{\zeta_1(\mathbf{r}, t) \mathbf{v}_1(\mathbf{r}, t)} = 2 \text{Re}[\xi(\mathbf{r}) \mathbf{V}^*(\mathbf{r})]$ and $\overline{\Omega_1(\mathbf{r}, t) \mathbf{v}_1(\mathbf{r}, t)} = 2 \text{Re}[\Omega(\mathbf{r}) \mathbf{V}^*(\mathbf{r})]$, where the complex amplitudes $U(\mathbf{r})$, $V(\mathbf{r})$, $\xi(\mathbf{r})$, and $\Omega(\mathbf{r})$ are given by Eqs. (B8)–(B11) and the asterisk denotes the complex conjugate.

We are further interested in obtaining the mean flow produced by a single particle, say, particle j . In this case, the integrals in Eqs. (B16) and (B17) for $\Phi_j(\mathbf{r})$ and $\Psi_j(\mathbf{r})$, and hence the mean velocity \mathbf{u}_j , can be evaluated explicitly. The time-averaged quantities computed for particle j read

$$\overline{\zeta_1 \mathbf{v}_1} = \frac{\omega}{16\pi} \frac{e^{-2\nu\gamma R_j}}{R_j} \cos^2(\varphi_j - \theta_j) (\cos \theta_j, \sin \theta_j),$$

$$\overline{\Omega_1 \mathbf{v}_1} = -\frac{\omega}{32\pi} \frac{e^{-2\nu\gamma R_j}}{R_j^2} \sin(2\varphi_j - 2\theta_j) (\cos \theta_j, \sin \theta_j).$$

With these expressions, the evaluation of integrals (B16) and (B17) results in

$$\Phi_j(\mathbf{r}) = \frac{\omega}{256\pi\gamma^2\nu^2} \frac{F_\Phi(\nu\gamma R_j)}{R_j^2} \cos(2\varphi_j - 2\theta_j), \quad (\text{B18})$$

$$\Psi_j(\mathbf{r}) = \frac{\omega}{768\pi\alpha\gamma\nu^2} \frac{F_\Psi(\nu\gamma R_j)}{R_j^2} \sin(2\varphi_j - 2\theta_j), \quad (\text{B19})$$

with $F_\Phi(x) = -1 + (1 + 2x + 2x^2 - 4x^3)e^{-2x} + 8x^4 E_1(x)$, $F_\Psi(x) = -3 + (3 - 2x + 2x^2 - 4x^3)e^{-2x} + 8x^4 E_1(x)$, and $E_1(x) = \int_x^\infty e^{-t} t^{-1} dt$.

APPENDIX C: TIME-AVERAGED EQUATIONS FOR THE MOTION OF PARTICLES

To obtain effective equations describing the motion of the particles, we have to average Eqs. (3) and (4) over time. As in the method of averaging [29] (see also Ref. [30]) we represent

the positions and orientations of the particles as

$$\mathbf{r}_j(t) = \mathbf{q}_j(t) + \delta\mathbf{q}_j(t), \quad \phi_j(t) = \varphi_j(t) + \delta\varphi(t), \quad (\text{C1})$$

where the contributions $\mathbf{q}_j(t)$ and $\varphi_j(t)$ describe the time-averaged or slow evolution of particles and $\delta\mathbf{q}_j(t) = \delta\mathbf{r}_j e^{i\omega t} + \text{c.c.}$ and $\delta\varphi_j(t) = \Delta_j e^{i\omega t} + \text{c.c.}$ stand for the time-periodic counterparts oscillating with the frequency ω , which are further represented via the complex amplitudes $\delta\mathbf{r}_j$ and Δ_j .

Note that on the right-hand side of Eqs. (3) and (4), we have such quantities as $\mathbf{v}(\mathbf{r}_j, t)$ and $\nabla h(\mathbf{r}_j, t) = \nabla \zeta(\mathbf{r}_j, t)$, to be taken at the instant position $\mathbf{r}_j(t)$. Making use of representation (C1) and the fact that the oscillating part $\delta\mathbf{q}_j$ is small compared to the mean part $\mathbf{q}_j(t)$, we can approximately write

$$\mathbf{v}(\mathbf{q}_j + \delta\mathbf{q}_j, t) \approx \mathbf{v}(\mathbf{q}_j, t) + \delta\mathbf{q}_j(t) \cdot \nabla \mathbf{v}(\mathbf{q}_j, t), \quad (\text{C2})$$

$$\zeta(\mathbf{q}_j + \delta\mathbf{q}_j, t) \approx \zeta(\mathbf{q}_j, t) + \delta\mathbf{q}_j(t) \cdot \nabla \zeta(\mathbf{q}_j, t) \quad (\text{C3})$$

and proceed to the time averaging. We describe the minimal model necessary to obtain the slow evolution of particle positions and orientations.

1. Time-averaged equations for the positions of particles

To be able to obtain the time-averaged equation for the positions of the particles, we first need to determine the complex amplitude $\delta\mathbf{r}_j$, which determines the oscillating contribution $\delta\mathbf{q}_j(t)$. For simplicity, we do this independently for the Stokes drag and for the gravitational term, as described below. In both situations, we neglect the interactions with other particles, which keeps our model simple and captures the basic physics. After we have found the complex amplitudes $\delta\mathbf{r}_j$, we are able to perform the time averaging and to obtain the corresponding contributions to the time-averaged equation for the positions of the particles.

a. Stokes drag term

As mentioned above, to determine the complex amplitude $\delta\mathbf{r}_j^{(S)}$ caused by the Stokes drag, we retain this term and neglect all other terms on the right-hand side of Eq. (3). Because $\delta\mathbf{q}_j$ is small, strictly speaking of order ϵ , we retain the leading term for \mathbf{v} in Eq. (C2) and taking into account Eq. (8b), we arrive at the equation

$$m\delta\ddot{\mathbf{q}}_j^{(S)} + \mu_t\delta\dot{\mathbf{q}}_j^{(S)} = \mu_t\mathbf{v}_1(\mathbf{q}_j, t).$$

We recall that $\delta\mathbf{q}_j^{(S)}(t) = \delta\mathbf{r}_j^{(S)} e^{i\omega t} + \text{c.c.}$ and $\mathbf{v}_1(\mathbf{q}_j, t) = \mathbf{V}(\mathbf{q}_j) e^{i\omega t} + \text{c.c.}$ to obtain

$$\delta\mathbf{r}_j^{(S)} = \frac{\mu_t \mathbf{V}(\mathbf{q}_j)}{-m\omega^2 + i\omega}. \quad (\text{C4})$$

With this result, we can evaluate the mean (time-averaged) contribution made by the Stokes drag to the time-averaged equation. Averaging Eq. (3) over time with all the terms on the right-hand side neglected, except for the Stokes drag, we have

$$m\ddot{\mathbf{q}}_j + \mu_t\dot{\mathbf{q}}_j = \mu_t\mathbf{u}(\mathbf{q}_j) + \mathbf{s}^{(S)}(\mathbf{q}_j), \quad (\text{C5})$$

where the right-hand side is determined by the velocity field as in Eq. (C2) averaged over time. Note that for a given particle j , we take into account the flow fields generated by all other

particles,

$$\mathbf{u}(\mathbf{q}_j) = \sum_{k \neq j} \mathbf{u}_k(\mathbf{q}_j), \quad \mathbf{s}^{(S)}(\mathbf{q}_j) = \sum_{k \neq j} \mathbf{s}_k^{(S)}(\mathbf{q}_j). \quad (\text{C6})$$

Here \mathbf{u}_k is the mean flow field produced by particle k evaluated via the potential $\Phi_k(\mathbf{q}_j)$ and the stream function $\Psi_k(\mathbf{q}_j)$, as given by Eqs. (B18) and (B19), at the position \mathbf{q}_j of particle j . Using Eq. (C4), the Stokes drift vector $\mathbf{s}_k^{(S)}(\mathbf{q}_j) = \mu_r \delta \mathbf{q}_k^{(S)}(t) \cdot \nabla \mathbf{v}_1^{(k)}(\mathbf{q}_j, t) = \mu_r [\delta \mathbf{r}_k^{(S)} \cdot \nabla \mathbf{V}_k^*(\mathbf{q}_j) + \text{c.c.}]$ is evaluated to yield

$$\mathbf{s}_k^{(S)} = -\frac{2m\mu_r^2}{m^2\omega^2 + \mu_r^2} \text{Re} \left\{ \left(1 + \frac{i}{m\omega} \right) \mathbf{V}_k \cdot \nabla \mathbf{V}_k^* \right\}, \quad (\text{C7})$$

where $\mathbf{V}_k(\mathbf{q}_j) = (U_k, V_k)$ are the complex amplitudes of the first-order velocity field $\mathbf{v}_1^{(k)}(\mathbf{q}_j, t)$ given by expressions (B8) and (B9) evaluated at \mathbf{q}_j . The subscript and superscript k implies that only the term with $j = k$ is retained in the sum. Physically this means that we evaluate the fields produced by particle k at the position of particle j .

b. Gravitational term

Similar to the consideration in Sec. IV, instead of the Stokes drag we now consider the gravitational term on the right-hand side of Eq. (3). The complex amplitude $\delta \mathbf{r}_j^{(G)}$ caused by the gravitational term can be determined from the equation

$$m\delta \ddot{\mathbf{q}}_j^{(G)} + \mu_r \delta \dot{\mathbf{q}}_j^{(G)} = -\beta \zeta_1(\mathbf{q}_j, t),$$

leading to

$$\delta \mathbf{r}_j^{(G)} = -\frac{\beta \nabla \xi(\mathbf{q}_j)}{-m\omega^2 + i\omega} \quad (\text{C8})$$

with $\xi(\mathbf{q}_j)$ being the complex amplitude of the field $\zeta_1(\mathbf{q}_j, t)$.

The time averaging of the corresponding equation gives us

$$m\ddot{\bar{\mathbf{q}}}_j + \mu_r \dot{\bar{\mathbf{q}}}_j = -\beta \nabla \overline{\zeta_2}(\mathbf{q}_j) + \mathbf{s}^{(G)}(\mathbf{q}_j) \quad (\text{C9})$$

with

$$\overline{\zeta_2}(\mathbf{q}_j) = \sum_{k \neq j} \overline{\zeta_2^{(k)}}(\mathbf{q}_j), \quad \mathbf{s}^{(G)}(\mathbf{q}_j) = \sum_{k \neq j} \mathbf{s}_k^{(G)}(\mathbf{q}_j). \quad (\text{C10})$$

We note that the term proportional to $\overline{\zeta_2}$ can be further neglected. By means of Eq. (C8), the Stokes drift vector caused by gravity $\mathbf{s}_k^{(G)}(\mathbf{q}_j) = -\beta \nabla [\delta \mathbf{q}_k^{(G)}(t) \cdot \nabla \zeta_1^{(k)}(\mathbf{q}_j, t)] = -\beta \nabla [\delta \mathbf{r}_k^{(G)} \cdot \nabla \xi_k^*(\mathbf{q}_j) + \text{c.c.}]$ is found to be

$$\mathbf{s}_k^{(G)}(\mathbf{q}_j) = -\frac{2m\beta^2}{m^2\omega^2 + \mu_r^2} \nabla |\nabla \xi_k(\mathbf{q}_j)|^2. \quad (\text{C11})$$

Here $\xi_k(\mathbf{q}_j)$ is the complex amplitude of the first-order field $\zeta_1^{(k)}(\mathbf{q}_j, t)$ given by expression (B10) evaluated at \mathbf{q}_j with a single term $j = k$ in the sum.

2. Time-averaged equation for the orientation of particles

The time averaging of Eq. (4) for the orientation of particles is straightforward. Taking into account decomposition (C1), for the time-averaged quantities we obtain

$$I\ddot{\bar{\phi}}_j + \mu_r \dot{\bar{\phi}}_j = T_j + \kappa H_0 [\nabla H(\mathbf{q}_j) \times \mathbf{P}_j] \cdot \hat{\mathbf{e}}_z, \quad (\text{C12})$$

with

$$H(\mathbf{q}_j) = \sum_{k \neq j} \overline{\sin(\omega t) \zeta_1^{(k)}(\mathbf{q}_j)} = -\sum_{k \neq j} \text{Im}\{\xi_k(\mathbf{q}_j)\}. \quad (\text{C13})$$

Here again $\xi_k(\mathbf{q}_j)$ is evaluated in the same way as in Eq. (C7).

-
- [1] M. C. Cross and P. C. Hohenberg, *Rev. Mod. Phys.* **65**, 851 (1993).
- [2] I. S. Aranson and L. Kramer, *Rev. Mod. Phys.* **74**, 99 (2002).
- [3] A. Snezhko, *J. Phys.: Condens. Matter* **23**, 153101 (2011).
- [4] I. S. Aranson, *Phys. Usp.* **56**, 79 (2013).
- [5] G. Whitesides and B. Grzybowski, *Science* **295**, 2418 (2002).
- [6] J. E. Martin, *Phys. Rev. E* **79**, 011503 (2009); K. J. Solis and J. E. Martin, *J. Appl. Phys.* **111**, 073507 (2012).
- [7] S. C. Glotzer and M. J. Solomon, *Nat. Mater.* **6**, 557 (2007).
- [8] I. S. Aranson and L. S. Tsimring, *Rev. Mod. Phys.* **78**, 641 (2006); *Granular Patterns* (Oxford University Press, Oxford, 2009).
- [9] N. Osterman, I. Poberaj, J. Dobnikar, D. Frenkel, P. Zihlerl, and D. Babić, *Phys. Rev. Lett.* **103**, 228301 (2009); M. Oettel and S. Dietrich, *Langmuir* **24**, 1425 (2008).
- [10] M. Leunissen, H. R. Vutukuri, and A. van Blaaderen, *Adv. Mater.* **21**, 3116 (2009).
- [11] N. Aubry, P. Singh, M. Janjua, and S. Nudurupati, *Proc. Natl. Acad. Sci. USA* **105**, 3711 (2008).
- [12] G. Vernizzi and M. Olvera de la Cruz, *Proc. Natl. Acad. Sci. USA* **104**, 18382 (2007).
- [13] M. V. Sapozhnikov, Y. V. Tolmachev, I. S. Aranson, and W.-K. Kwok, *Phys. Rev. Lett.* **90**, 114301 (2003).
- [14] J. Yan, M. Bloom, S. C. Bae, E. Luijten, and S. Granick, *Nature (London)* **491**, 578 (2012).
- [15] J. Dobnikar, A. Snezhko, and A. Yethiraj, *Soft Matter* **9**, 3693 (2013).
- [16] S. Jäger, H. Stark, and S. H. L. Klapp, *J. Phys.: Condens. Matter* **25**, 195104 (2013).
- [17] R. Dreyfus, J. Baudry, M. L. Roper, M. Fermigier, H. A. Stone, and J. Bibette, *Nature (London)* **437**, 862 (2005).
- [18] B. A. Grzybowski, M. Radkowski, C. J. Campbell, J. N. Lee, and G. M. Whitesides, *Appl. Phys. Lett.* **84**, 1798 (2004).
- [19] A. Snezhko, I. S. Aranson, and W. K. Kwok, *Phys. Rev. Lett.* **96**, 078701 (2006); *Phys. Rev. E* **73**, 041306 (2006).
- [20] A. Snezhko, I. S. Aranson, and W.-K. Kwok, *Phys. Rev. Lett.* **94**, 108002 (2005).
- [21] J. E. Martin, E. Venturini, J. Odinek, and R. A. Anderson, *Phys. Rev. E* **61**, 2818 (2000).
- [22] M. Belkin, A. Snezhko, I. S. Aranson, and W.-K. Kwok, *Phys. Rev. Lett.* **99**, 158301 (2007).

- [23] A. Snezhko, M. Belkin, I. S. Aranson, and W.-K. Kwok, *Phys. Rev. Lett.* **102**, 118103 (2009).
- [24] A. Snezhko and I. S. Aranson, *Nat. Mater.* **10**, 698 (2011).
- [25] M. Belkin, A. Glatz, A. Snezhko, and I. S. Aranson, *Phys. Rev. E* **82**, 015301 (2010).
- [26] D. L. Piet, A. V. Straube, A. Snezhko, and I. S. Aranson, *Phys. Rev. Lett.* **110**, 198001 (2013).
- [27] S. Shklyaev and A. V. Straube, *New J. Phys.* **10**, 063030 (2008); A. V. Straube, *J. Phys. Condens.: Matter* **23**, 184122 (2011).
- [28] A. Hucht, S. Buschmann, and P. Entel, *Europhys. Lett.* **77**, 57003 (2007).
- [29] A. H. Nayfeh, *Introduction to Perturbation Techniques* (Wiley, New York, 1981).
- [30] A. V. Straube, D. V. Lyubimov, and S. V. Shklyaev, *Phys. Fluids* **18**, 053303 (2006).